Polymer 50 (2009) 1577–1587

Contents lists available at ScienceDirect

Polymer

journal homepage: www.elsevier.com/locate/polymer

# Roles of graphite oxide, clay and POSS during the combustion of polyamide 6

Aravind Dasari [a,1], Zhong-Zhen Yu [b,*], Yiu-Wing Mai [a], Guipeng Cai [a], Huaihe Song [b]

[a] Centre for Advanced Materials Technology (CAMT), School of Aerospace, Mechanical and Mechatronic Engineering (J07), The University of Sydney, Sydney, NSW 2006, Australia
[b] Beijing Key Laboratory on Preparation and Processing of Novel Polymeric Materials, Department of Polymer Engineering, College of Materials Science and Engineering, Beijing University of Chemical Technology, Beijing 100029, China

ARTICLE INFO

*Article history:*
Received 16 September 2008
Received in revised form
18 January 2009
Accepted 22 January 2009
Available online 29 January 2009

*Keywords:*
Flame retardancy
Nanocomposites
Polyamide

ABSTRACT

Two contrasting approaches have been adopted in the current study to obtain *environmental benign* and *superior flame retardant polymer nanocomposites*. In the first approach, polyhedral oligomeric silsesquioxane (POSS) is incorporated as an additional filler in polyamide 6/clay nanocomposite to improve the homogeneity of the 'physical' barrier, since POSS transforms to a glassy material upon fire and enhances the coupling of silicate layers to each other. In the second approach, fire response of an intumescent system, polyamide 6/graphite oxide (GO), is compared to polyamide 6/clay systems. The intention of using GO as a flame retardant is to benefit from its layered structure ('physical' barrier mechanism) and intumescent/blowing effect ('chemical' mechanism). Considerable insight and physical knowledge on the roles of different fillers in the combustion process have been obtained, which would provide useful guidance for the development of a new generation of nanocomposites. Besides the obvious contrasting differences in the flame properties of different materials, the incorporation of various fillers, depending on their nature, has both advantages and disadvantages from the viewpoint of flame retardancy.



## 1. Introduction

Theoretically, complete protection against fire for a polymeric material when used for automotive, structural or other applications is possible [1–3] by: (a) reducing the heat evolved to below that required to sustain combustion, (b) isolating the flame from the oxygen, (c) reducing the heat flow back to the polymer to prevent further pyrolysis, and (d) introducing flame retardant compounds. Practically, however, many serious problems persist in every mechanism mentioned, which makes it impossible for complete protection (under forced combustion) against fire. Further taking into account eco-friendliness, ultimate mechanical and physical properties required for end applications and processing difficulties [1–7], use of nanoclay as a fire retardant in polymers seems to be a better option [8–12]. This is because even at low clay loading with no additional flame retardants in the system, heat release rates (HRRs) and mass loss rates (MLRs) were greatly reduced compared to corresponding neat polymers. This was attributed to the structural collapse of the nanocomposite during combustion and formation of a multi-layered carbonaceous-silicate barrier on the polymer surface.

Nevertheless, the main disadvantage of polymer/clay nanocomposites is that they do not extinguish and burn slowly until most of the fuel has been burnt. As a result, these materials by themselves are unable to meet the requirements of the ignition resistance tests (e.g. vertical burning UL94). It is also important that the objective should be to thoroughly understand and develop eco-friendly and superior flame retardant polymer/layered silicate nanocomposites and not just to pass the fire testing standards. This is due to the differences in various testing standards; for example, short-term (UL94 test which is the major criterion for most commercially available fire retardants) versus long-term (cone calorimeter, a bench-scale test to simulate real-world fire conditions) fire exposure conditions. It has been reported that some polymers, particularly polypropylene and polyamides using melamine or combination of melamine and clay layers as fillers pass the UL94 test with a V-rating by extinguishing the fire [2,13,14]. However, the primary mechanism for this is dripping; that is, they drip away from the flame. So, despite passing the testing standard, this material is not an ideal choice as it may burn completely if exposed to long-term flame conditions.

Based on physical evidences provided in our recent work on flame retardancy of highly-filled polymer/clay nanocomposites [10], it was concluded that all the clay layers were not migrating to the burning surface resulting in apertures/openings in the char

* Corresponding author. Tel./fax: +86 10 6442 8582.
*E-mail address:* yuzz@mail.buct.edu.cn (Z.-Z. Yu).
[1] Current address: Madrid Institute for Advanced Studies of Materials (IMDEA-Materials), E.T.S. de Ingenieros de Caminos, 28040 Madrid, Spain.

0032-3861/$ – see front matter © 2009 Elsevier Ltd. All rights reserved.
doi:10.1016/j.polymer.2009.01.050

where burning of polymer continued. To combat this problem, four approaches were suggested and one of which was to add inorganic additives like glass or zinc borate to a polymer/clay nanocomposite. It was assumed that these compounds transform to a partially ceramic-like material and improve the coupling of silicate layers upon fire so that the openings/apertures in the char could be reduced. It is one of the objectives of the current study to incorporate polyhedral oligomeric silsesquioxane (POSS) as additional filler in polyamide 6/clay nanocomposite and understand its flame response. POSS molecules have hybrid (organic–inorganic) architecture and their structure contains a stable inorganic Si–O core, which is intermediate between silica and silicones [15–20]. This core is covered externally by organic substituents which can be modified to yield a wide range of polarities and functionalities [15–25]. This great variety gives a diversity of silsesquioxanes.

The response noted in the literature on flame performance of polymers with POSS as nano-filler is mixed and depends on their structure and nature of the functional groups attached to them. Generally, POSS compounds when subjected to combustion produce a thermally insulating and oxidatively stable silicon oxycarbide 'black glass' (Si–O–C ceramic char), which would act as an insulating barrier [15,17,19,23,26]. But, even in those studies which showed improvements in fire properties with POSS, poor stability, incoherency and discontinuity/non-uniformity of the char always gave minimum reductions in flame properties compared to the clay nanocomposites. In the present study, however, POSS is expected to play only a secondary role in supporting the silicate char by coupling the layers together.

In addition, in this work, an intumescent system, polyamide 6/graphite oxide (GO) composite was prepared and its fire response/efficiency compared to the polyamide 6/organoclay system. In intumescent (and blowing) flame systems, the material swells and evolves gaseous agents (and consumes heat) when it is exposed to fire to form a porous foamed mass, usually carbonaceous, that acts as a barrier to interrupt the combustion of a polymer [27]. GO is a pseudo 2D solid-like layered compound where carbon atoms within the layered nano-sheets form hexagonal cells through covalent bonds; and the carbon layers are joined to each other by weak Van der Waals forces. GO has some oxidants like sulphuric acid, hydrogen peroxide and/or potassium permanganate inserted between the carbon layers of graphite and has various functional groups on it, including hydroxyl, carbonyl and epoxy. It is shown to be a very efficient intumescent agent as it acts both as a carbonization compound and a blowing agent [27–32]. According to Camino et al. [33], the expansion of GO occurs by a redox reaction Eq. (1) between sulphuric acid and graphite that originates the blowing:

$$C + 2H_2SO_4 \rightarrow CO_2\uparrow + 2H_2O\uparrow + 2SO_2\uparrow \quad (1)$$

During the voluminous expansion, lamellar structure of GO particles is transformed to a vermicular structure and exfoliates along the *c*-axis of a graphite crystal. It has also been reported that ~10 wt.% of blowing agent (water) is given off at 600 °C [27].

Recently, many studies were reported using GO as a flame retardant in different polymers and obtained a positive response of decrease in HRR (and MLR) [28–30,34,35]. As expected, the release of water and graphite expansion suffocates the flames and the char layer limits the heat and mass transfer from the polymer to the heat source. So, it would be interesting to compare the flame performance of GO and clay, both having a layered structure but based on different mechanisms to retard fire; clay mainly depends on the collapse of its structure and formation of a 'physical' barrier; whereas GO depends on both chemical and physical mechanisms.

## 2. Experimental work

### 2.1. Preparation of materials

Polyamide 6 with a trade name of Ultramid B3S was obtained from BASF (Germany) via Marplex (Australia) Pty Ltd. Organoclay having a cation exchange capacity of 90 mequiv/100 g (trade name: Cloisite® 30B) was obtained from Southern Clay Products Inc. (USA) via Jim Chambers & Associates, Australia. The alkyl ammonium surfactant used in the organoclay was methyl, tallow, bis-2-hydroxyethyl quaternary ammonium chloride. Graphite oxide with an average particle size of ~180 μm (80 mesh) was supplied by Laixi Fanrong Graphite Factory (China). It was prepared by oxidizing natural flake graphite with a mixture of concentrated sulphuric acid and hydrogen peroxide. Wide-angle X-ray diffraction (XRD) pattern of as-received GO, however, revealed that except for a broad and low intensity peak at $2\theta \sim 13.6^\circ$ (interlayer spacing ~ 0.65 nm), no considerable expansion occurred in the gallery space of graphite layers during oxidation as a sharp and high intensity original graphite peak at $2\theta \sim 26.6^\circ$ (interlayer spacing ~0.335 nm) was still evident. Tri-silanol-phenyl POSS (Scheme 1) was supplied by Hybrid Plastics, Inc. (USA) and used as-received. It possesses a hybrid 3D partial cage-like structure with one corner Si missing, leaving three silanol (Si–OH) functional groups. The presence of silanol groups (Si–OH) is expected to enhance the particle–polymer interactions.

Polyamide 6 pellets, organoclay, POSS, and GO were oven-dried at 85 °C for 24 h. Then, the desired proportions were mixed and melt-compounded in a Werner & Pfleiderer ZSK-30 twin-screw extruder ($L/D = 30$, $L = 0.88$ m). Extrusion was performed within the temperature range of 210–245 °C and a screw speed of 300 rpm. The extruded pellets were oven-dried and molded into standard $100 \times 100 \times 3$ mm$^3$ plates using a Netstal HP1000 injection molding machine with the barrel and mold temperatures maintained at 240 and 50 °C, respectively. The holding pressure was 60 MPa; while the holding and cooling times were 10 and 25 s, respectively. The following materials were prepared using these conditions: neat polyamide 6 – B0, polyamide 6/POSS (85/15) nanocomposite – B1, polyamide 6/organoclay (85/15) nanocomposite – B2, polyamide 6/POSS/organoclay (70/15/15) nanocomposite – B3 and polyamide 6/GO (85/15) composite – B4.

### 2.2. Morphology observations

To study the microstructures of these nanocomposites, ultrathin sections of ~70–90 nm in thickness were cryogenically cut with a diamond knife in a liquid nitrogen environment at −100 °C using a Leica Ultracut S cryo-microtome. Sections were collected on the holey formvar/carbon coated 400-mesh copper grids. Then, the

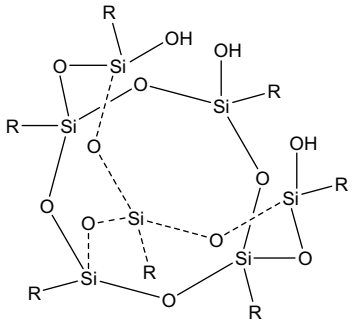


**Scheme 1.** Structure of tri-silanol-phenyl polyhedral oligomeric silsesquioxane, $C_{42}H_{38}O_{12}Si_7$.

thin sections were observed with a Philips CM12 transmission electron microscope (TEM) at an accelerating voltage of 120 kV. For B4, a Philips S-505 scanning electron microscope (SEM) was also used to observe the dispersion of GO after freeze-fracturing an injection-molded bar in liquid $N_2$.

### 2.3. Thermal and combustion testing

Thermogravimetric analysis (TGA) was conducted on TA Instruments (TGA 2950) from ambient (~25 °C) to 800 °C at a rate of 20 °C/min in nitrogen and the weight loss/temperature curves were monitored. Combustion tests were performed in a cone calorimeter (CSIRO, Ryde, Australia) on injection-molded plates at an incident heat flux of 50 kW/m$^2$. The instrument was capable of recording ignition times, heat release and mass loss rates, specific extinction area, CO and $CO_2$ yields. All sides of the samples were wrapped in aluminum foil except for the upper face, which was exposed to the heat flux.

### 2.4. X-ray diffraction

A Siemens D5000 X-ray diffractometer with Cu Kα radiation ($\lambda = 1.54$ Å) at a generator voltage of 40 kV and a current of 30 mA was used to study the diffraction behavior of the organoclay and polyamide 6 nanocomposites. All tests were conducted in reflection mode at ambient temperature with $2\theta$ varying between 1° and 30°. The scanning speed was 1 °/min and the step size was 0.05°. XRD patterns were also obtained after combustion testing of the nanocomposites from the surfaces of the residues. Further, a Shimadzu S6000 X-ray diffractometer with Cu Kα radiation ($\lambda = 1.54$ Å) at a generator voltage of 40 kV and a current of 30 mA was used to characterize the diffraction behavior of different materials at various temperatures in nitrogen. The sample was placed on a copper block inside a variable-temperature attachment where the temperature was electronically controlled, heated at 20 °C/min to the desired temperature and held for 5 min before data collection. All experiments were carried out with a scanning speed of 3 °/min and a step size of 0.04°.

### 2.5. Characterization of residues

In addition to the XRD analyses, optical, SEM and TEM were used to characterize the residues of the burnt samples. The flame exposed surfaces were examined with SEM and a digital camera to obtain information of the continuity of the protective layer, while the cross-sections beneath the surfaces of the combustion residues were observed via TEM to identify the uniformity and thickness of the insulating layer so as to gain insights on the mechanisms of flame retardancy.

## 3. Results and discussion

### 3.1. Morphology and structure

Before discussing the TEM observations, it should be noted that XRD analyses of all material systems were performed. For binary polyamide 6/organoclay nanocomposite (B2), it was revealed that except for the peak corresponding to the γ-crystalline phase of polyamide 6 ($2\theta \sim 21.4°$), no other peaks were found in the $2\theta$ range 1–30°. In the binary polyamide 6/POSS system (B1), though the γ-crystalline phase of polyamide 6 at $2\theta \sim 21.4°$ is strong, the low intensity reflection peaks at $2\theta \sim 20.3°$ and ~23.3° corresponding to the diffraction of (100) and (010, 110) crystal planes of polyamide 6 (in α-crystalline phase) were also seen suggesting a mixture of different phases. While in ternary nanocomposite (B3), like B2, only strong diffraction peak corresponding to γ-crystalline phase of polyamide 6 is seen. Also, a diffraction peak at $2\theta \sim 7.83°$ ($d$-spacing ~1.13 nm) was observed in B1 and B3, which is a typical crystal peak of POSS with similar structure [15,22]. This indicates that separate POSS domains in crystalline phase are present in these materials. In polyamide 6/GO composite, apart from the original graphite peak at $2\theta \sim 26.6°$, another peak (though of lower intensity) at $2\theta \sim 2.59°$ (corresponding to an interlayer spacing of ~3.41 nm) is observed. This suggests that some intercalation of polymer into graphite layers occurred during the melt-compounding process. Also, peaks corresponding to the α-crystalline phases of polyamide 6 are seen.

Typical TEM micrographs of binary polyamide 6/organoclay and ternary polyamide 6/POSS/organoclay nanocomposites are shown in Fig. 1a and b, respectively. Both micrographs are taken from the cross-section of the injection-molded thin plates along a plane parallel to the flow direction. Clay layers, as expected, based on our previous study, in B2 are well dispersed, finely distributed, and in addition highly oriented with their planar dimensions along the injection molding direction. Even in the ternary nanocomposite, the additional incorporation of POSS had no significant influence on the dispersion quality of the organoclay platelets which are finely dispersed and highly oriented in the polyamide matrix. In line with the XRD results, POSS domains are evident in the nanocomposite and in the nano- to sub-micron scale. Except for some POSS domains where the presence of organoclay layers are seen (pointed with arrows in Fig. 1b), most of them are dispersed separately in the polymer matrix; but are highly oriented along the flow direction. Size distribution analysis of the POSS particles using 'Image J' (from the National Institutes of Health, USA) on the TEM micrographs revealed that the mean sizes along the major and minor axis of particles were 220 and 115 nm, respectively. While the standard deviations were 36 and 20 nm along the major and minor axis, respectively, suggesting a broad size distribution. A minimum of 500 POSS particles were considered for these calculations. In the binary polyamide 6/POSS nanocomposite, POSS domains are present at the sub-micron level similar to those in the ternary nanocomposite (and therefore TEM micrographs are not shown here). The mean sizes (and standard deviations) of POSS particles in the binary nanocomposite along their major and minor axis were 310 (45) nm and 250 (38) nm, respectively. Although pure molecular dispersion of POSS has been observed in some thermosets [36,37], in the majority of cases, it has been reported that POSS domains often form as POSS undergoes self-aggregation in competition with both chemical bonding to, and molecular dispersion in, the matrix. In polyamide 6/GO composite, a mixed dispersion is observed with the presence of both original graphite units (consisting of few graphene sheets, Fig. 1c) and some delaminated graphene sheets in polyamide 6 (Fig. 1d), supporting the XRD results.

### 3.2. Thermogravimetric analysis

As noted in our previous work [10] and other studies [38–41], the major disadvantage of modifying the clay layers with low molecular weight alkyl ammonium (organic) surfactants is that they are thermally unstable and decompose usually from ~180 °C. This is much lower than the processing temperature of most engineering polymers and thus adversely affects the thermal stability despite enhancing the compatibility of clay layers with polymers. As shown in Fig. 2a, thermal decomposition of organoclay powder can be divided into four stages, starting with loss (or evolution) of free (absorbed) water residing between montmorillonite crystallites and gaseous species at ~180 °C (Stage I). Although organoclay is considered hydrophobic, due to the alkyl

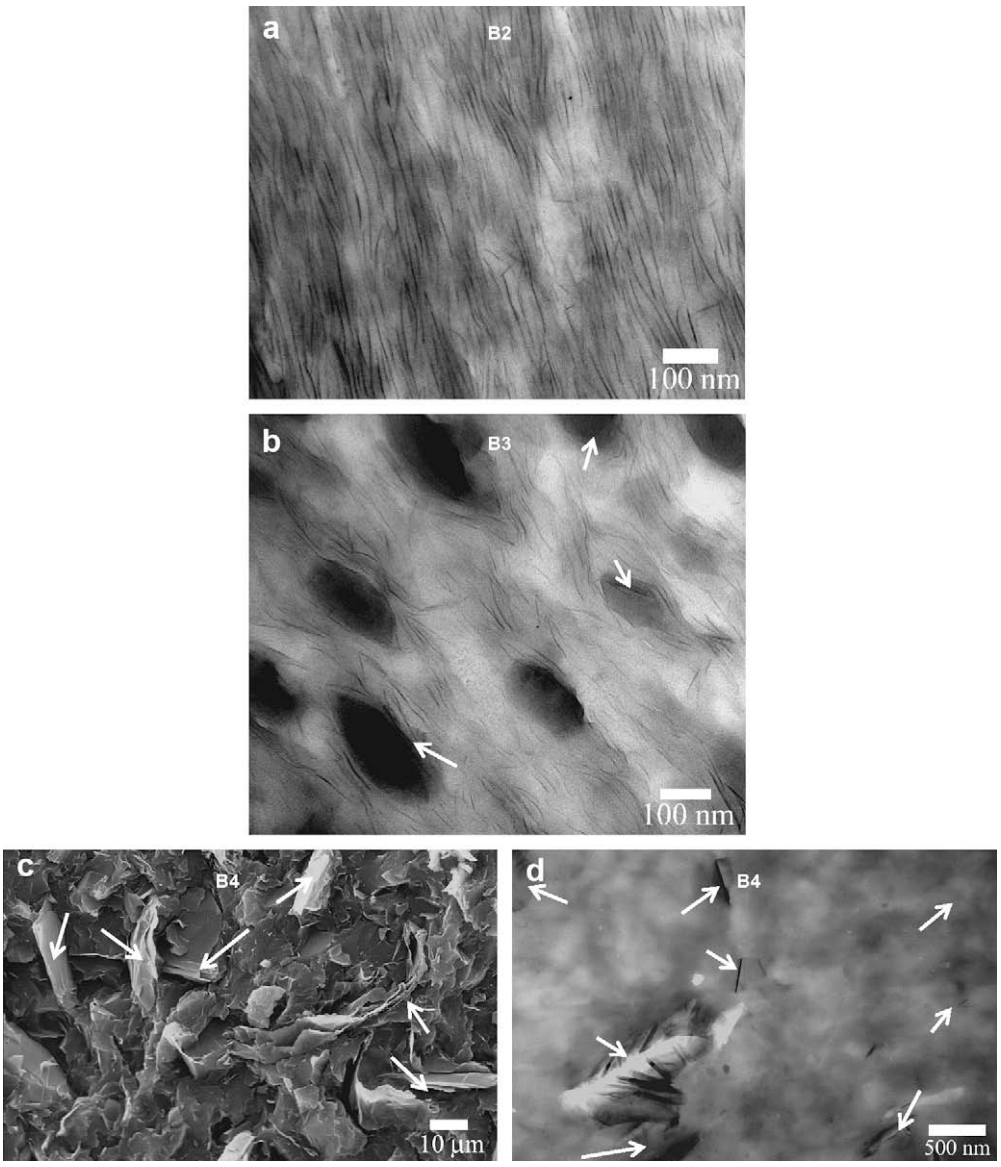


**Fig. 1.** TEM (a–b, d) and SEM (c) micrographs showing the dispersion quality of (a) organoclay layers in B2; (b) organoclay layers and POSS particles in B3; (c–d) graphite sheets in B4. The arrows in: (b) point to the presence of some clay layers in the POSS particles, (c) indicate the presence of original graphite particles (consisting of a few graphene sheets), and (d) point to the presence of fine and delaminated nano-sheets of graphite.

ammonium cations, water absorption still occurs on the exterior of the aggregates and along the hydrophilic layer edges depending on the environmental conditions [39]. This is followed by the decomposition and evolution of organic substances between ~200 and 470 °C (Stage II); then, dehydroxylation of aluminosilicate lattice occurs from 470 to 700 °C (Stage III); and finally, evolution of products associated with residual organic carbonaceous matter occurs from 700 °C (Stage IV).

The thermal decomposition process of GO can be divided into three stages as noted in Fig. 2a. The first stage is around ~100 °C due to the loss of free water from the GO sheets; second stage is where significant weight loss occurs starting at ~200 °C and continues to ~250 °C. During this stage, GO loses a huge ~55% of its weight owing to the decomposition of the oxygen and carbonyl functional groups in the GO layer. This means the voluminous expansion process of GO is mostly occurring during this stage, which leads to a critical question of its flame performance when used in polyamides as their processing temperature is above 240 °C. Therefore, it seems that most of the expansion occurs *in situ* during processing in the extruder. This is certainly beneficial in terms of delamination of the sheets (by this *in situ* process); but is disadvantageous in terms of flame performance as an intumescent fire retardant. The last stage in the thermal decomposition process is related to the combustion of the carbon skeleton of GO [32]. After the three decomposition stages, the final char yield is only ~40%.

Compared to organoclay and GO, as expected, POSS seems to have better thermal stability up to 400 °C (Fig. 2a) though the final char yield is similar to that of organoclay (~73%). However, flame performance of the nanocomposites with POSS is poor compared to those organoclay reinforced materials (see below, Section 3.4). The initial high thermal stability of POSS (to ~400 °C) is determined by its chemical structure, such as the bond energy, type of molecules and reactivity of the bonds. The higher bond energy of Si–O, in particular, yields higher thermal stability. The decomposition process of tri-silanol-phenyl POSS includes the evolution of cyclic organosilanes starting at 400 °C, followed by the loss of

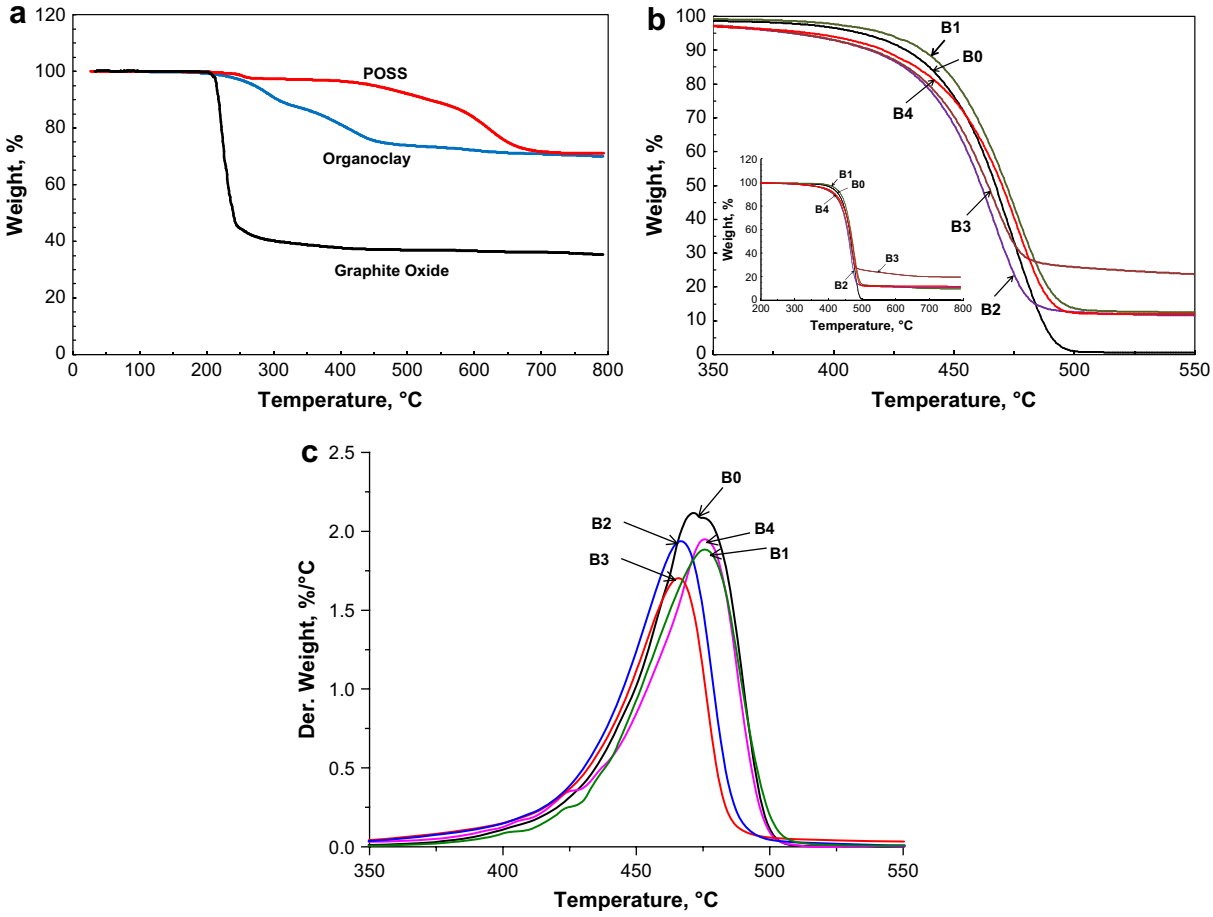


**Fig. 2.** (a) TGA plots of organoclay, POSS and GO powders; (b) TGA and (c) DTG curves of neat polyamide 6 (B0) and its composites (B1 to B4). The inset in (b) shows an extended *x*-axis.

hydrocarbon fragments between 450 and 550 °C, and finally POSS cage degradation between 550 and 680 °C producing a ~73% black glass residue.

Fig. 2b and c show TGA and DTG analysis of neat polyamide 6 (B0) and its binary and ternary nanocomposites (B1 to B4) in nitrogen. The dispersion/distribution of layered fillers in polyamide 6 did not have any positive effects on its thermal stability implying that the barrier properties of these high aspect ratio fillers are not the primary determining factors of thermal stability. Instead, as mentioned, organoclay and GO containing materials start to decompose earlier than the neat polymer. Only polyamide 6/POSS binary nanocomposite showed higher thermal stability than all the other materials. For example, 5% weight loss thermal degradation temperatures of B0 and B1 to B4 are ~411, 421, 382, 383, and 390 °C, respectively. The maximum decomposition temperatures (B0 ~473 °C; B1 ~476 °C; B2 ~466 °C; B3 ~465 °C; and B4 ~475 °C) obtained from the DTG curves (Fig. 2c), however, show little difference between different samples (although organoclay reinforced materials had ~10 °C lower maximum decomposition temperature than others). This indicates clearly that addition of different types of inorganic fillers (either 2D or 3D) is not always beneficial for improving the thermal stability of polyamide 6.

It was also reported that after the thermal decomposition of organic content through the Hoffman degradation reaction, the acidic clay site formed on the clay surface will have a direct interface with the remaining polymer [42], which is generally known to cause hydrocarbon cracking, further degrading the polymer [43]. Thus, the presence of large quantities of organic content and the catalytic activity of clay seems to be the reason for the poor thermal stability of the nanocomposites. While the intumescent and blowing nature of GO at relatively low temperature resulted in a faster and greater weight loss, the main decomposition steps were attributed to the dehydration and decarbonisation processes.

### 3.3. Response to fire exposure

Representative heat release rate curves of B0, B1 to B4 are shown in Fig. 3a. As expected, the presence of 2D layered fillers (B2 to B4) significantly reduced the heat release rates (and peak HRRs) compared to neat polyamide 6. But despite its good thermal stability compared to other materials, 3D domains of POSS containing polyamide 6 nanocomposite (B1) showed no reduction in the heat release rate curve compared to neat polyamide 6. The peak HRR of B0, B1 to B4 are 982, 999, 385, 389, 417 kW/m$^2$, respectively. Also, B2 to B4 experienced very much slower rate of combustion, i.e. delayed burning, while B0 and B1 burned quickly. The dramatic reductions in HRRs in B2 to B4 could not extinguish the flame (even in B4 where voluminous expansion is seen during burning) until most of the fuel has been burnt out; therefore, resulting in similar or in some cases slightly higher total heat released per unit area (due to the presence of thermally unstable organic content) compared to the neat polymer. The total heat release per unit surface area (integrated over time) for neat polyamide 6 is ~100 MJ/m$^2$; while for B1 to B4, they are 99, 101, 97 and 101 MJ/m$^2$, respectively.

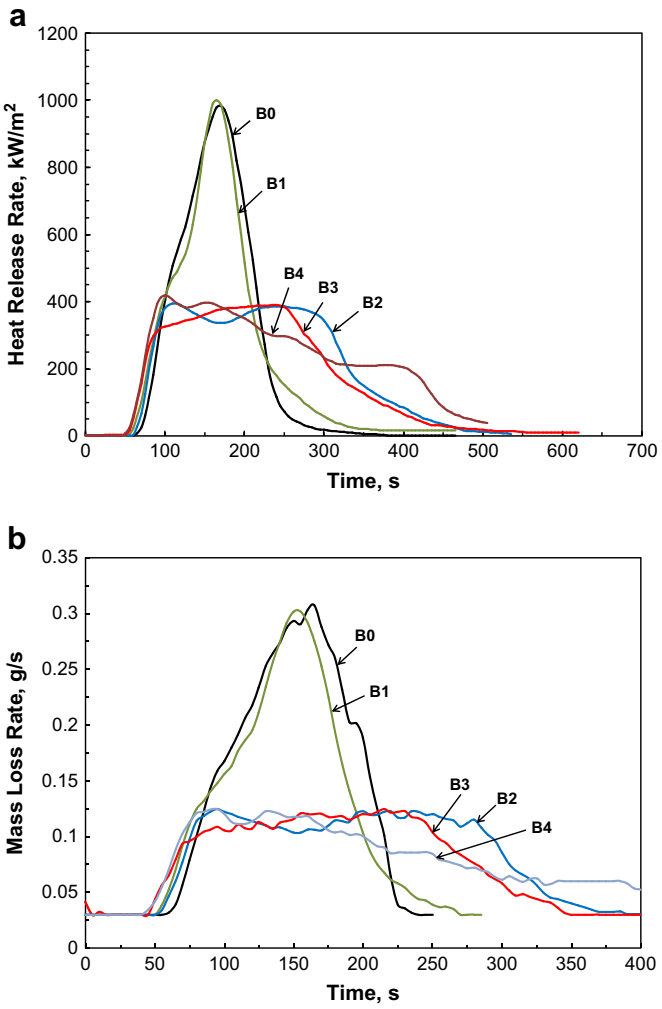


**Fig. 3.** Flammability properties of B0 and B1 to B4 evaluated with a cone calorimeter at an incident heat flux of 50 kW/m$^2$: (a) heat release rates (HRR) and (b) mass loss rates (MLR).

As indicated by the TGA results on thermal stability and, in line with them, time-to-ignition of the materials varied. Ignition of B4 occurred earlier (~55 s) followed by B3 (~57 s) and B2 (~60 s), and finally B1 (~64 s) and B0 (~65 s). The large amount of low molecular weight organic surfactants in clay reinforced materials seems to be responsible for the early ignition behavior of B2 and B3 materials. However, these differences definitely cannot outweigh subsequent performances of these materials under fire, which are far superior to B0 and B1 with slightly better ignition resistance. Besides organoclay reinforced materials, early ignition behavior was similarly observed in other systems consisting mostly of conductive fillers like carbon nano-tubes and graphite-based compounds [28,32,44–47]. The mechanism is attributed to the improved thermal conductivity in these materials; that is, the heat absorption by GO would give rise to higher thermal conductivity, and consequently, the temperature near each GO particle becomes high enough to initiate thermal degradation of the polymer in their vicinity, and hence reducing the ignition resistance. Another reason that can add to this is the oxidation of GO in flame representing a further contribution to heat flux radiated from the flame. This is also true for POSS where oxidation of the organic substituents on POSS is expected to occur.

Mass loss rate curves of all the samples plotted in Fig. 3b are proportional to the heat release rate curves and they indicate good fire performance of the materials having layered fillers. Of all the nanocomposites, the flame performance tested via cone calorimetry is poor for binary polyamide 6/POSS nanocomposite. As explained in Section 1, the fire response of the polymer/POSS nanocomposites by themselves (without any flame retardants) is mixed and depends on their structure and the nature of functional groups attached to them. These obviously different behaviors in the flame properties of B0, B1 to B4, particularly time-to-ignition versus heat release and mass loss rates indicate problems of characterizing the fire performances of materials using contrasting fire exposure techniques like short-term (UL94 tests) and long-term (cone calorimeter tests) conditions.

It is worth noting that visual observations during combustion experiments in the cone calorimeter revealed interesting behavior for neat polyamide 6 and its composites. Neat polyamide 6 was completely melted and accompanied by severe bubbling and bursting at the sample surface. At the end of the test, no residue was left behind. Binary polyamide 6/POSS system showed similar behavior in terms of severe bubbling and bursting as the neat polymer. Although it is thought that phenyl groups of POSS can easily form a non-combustible char and contribute to high char yield (due to the entrapment of carbon in the structure by phenyl group condensation [18]), only a non-continuous and patchy ceramic material from POSS degradation was left after combustion suggestive of an ineffective physical barrier to retard the combustion process. While in the presence of organoclay (B2 and B3), severe bubbling was not observed though some bubbling between cracks on the char (or island-like structures) was clearly seen. In contrast, in the presence of GO, the process of burning was entirely different. The voluminous expansion prevented bubbling and bursting at the surface and it resembled a perfect and continuous surface. Even so, flames were not seen at the top surface of the sample during combustion; but surprisingly, flames were observed from the lateral sides of the expanded material and continued until most of the fuel had been burnt out suggesting the creation of large cracks/openings along the normal axis of expansion from where the transfer of combustion products occurred.

### 3.4. Characterization of combustion residues

#### 3.4.1. Optical and SEM analysis

For B2, an optical and a typical SEM micrograph on the top surface of residue (which was exposed to flame) are shown in Fig. 4a–b, respectively. While many (shallow) cracks which give an impression of small discrete island-like structures are seen on the surface of the combustion residue, the char is physically rigid and integrated. SEM micrograph taken on an island-like structure shows the floccules indicating the swelling nature of the microstructure of the char; but more importantly, only some of them have opened up due to the bursting of bubbles (indicated by arrows). This suggests that locally in the island-like structures or away from the cracks, the physical barrier is stable and tightly packed. When POSS is further added, the residue surface microstructure is slightly different. In many places, island-like structures are seen similar to B2 (not shown here); but in some regions, the surrounding cracks appear to be closed, i.e. no gaps or openings can be seen between the island-like structures. This is possibly due to the additional support provided by the glass (ceramic char) residue. As mentioned before, POSS transforms to ceramic-like material upon fire and is expected to couple the silicate layers, thereby enhancing the structural integrity of the char by providing effectively a continuous coating or fill up the voids in the char. A representative photograph of this behavior is shown in Fig. 4c. However, as the performance of this material is not significantly different from binary organoclay nanocomposite, the additional

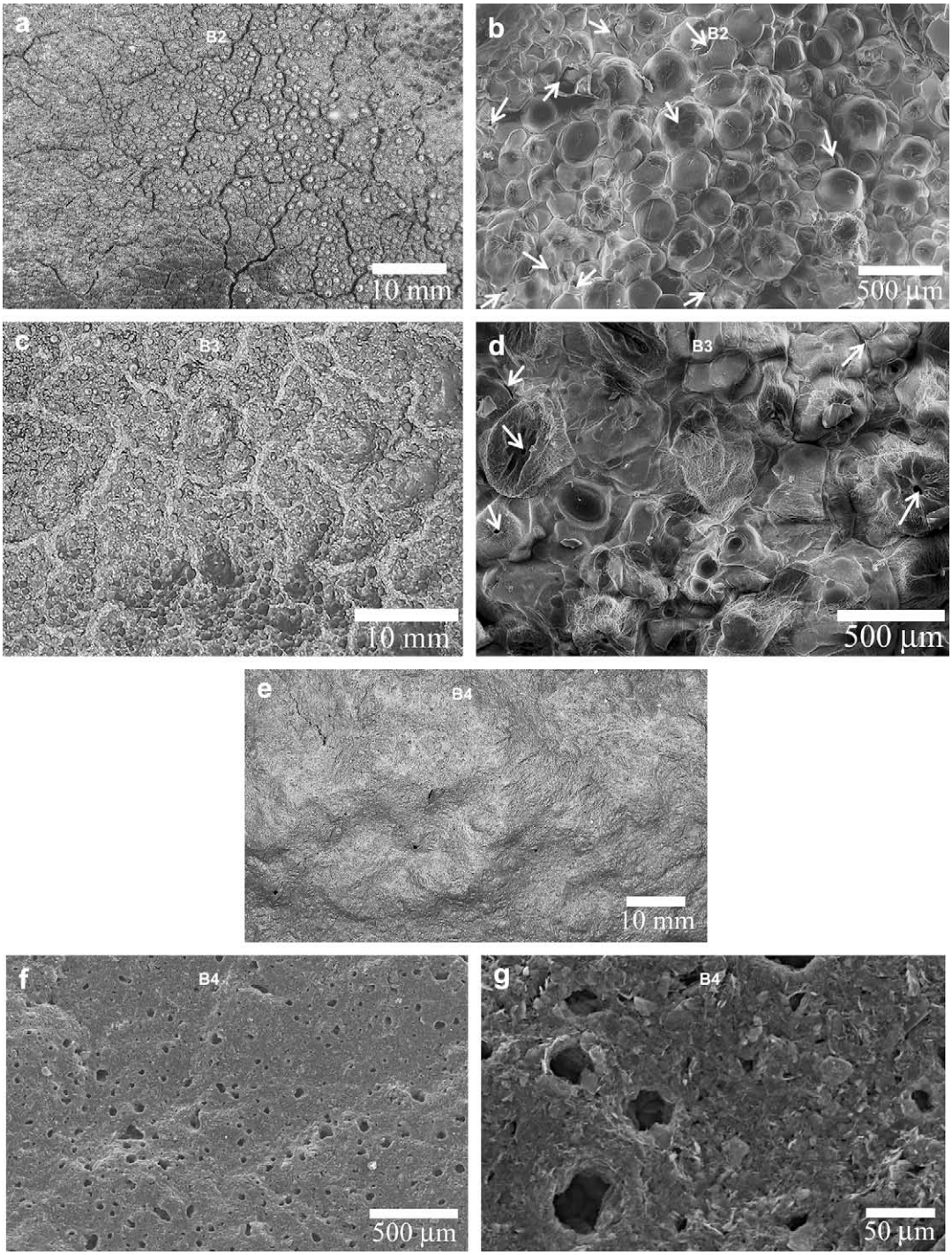


**Fig. 4.** Digital (a,c,e) and SEM (b,d,f,g) photographs of the residues left after combustion tests at an incident heat flux of 50 kW/m$^2$ for: (a–b) B2 – polyamide 6/organoclay (85/15); (c–d) B3 – polyamide 6/organoclay/POSS (70/15/15); and (e–g) B4 – polyamide 6/graphite oxide (85/15) nanocomposites. White arrows in (b) and (d) point to some of the opened floccules.

presence of POSS and the resulting surface microstructure (though only in some regions) of the residue does not seem to be beneficial. A typical SEM micrograph of the surface microstructure of the residue of B3 is shown in Fig. 4d. Although the surface morphology is slightly different from B2, floccules are still observed.

In contrast, the residue of polyamide 6/graphite oxide appears to be smooth, solid-like and continuous, without any major cracks (Fig. 4e). However, the char is physically extremely soft and even a puff of air could cause it to collapse. This suggests that even though the intumescent behavior of graphite oxide is useful for combating fire by delaying the fire-spread, the structural integrity is still questionable and obviously will not allow sufficient time for safety measures to be taken in practical situations. Also, at the micro-level, there are numerous voids ranging from a few nanometers to one or two hundred micrometers over the entire surface of the residue (even observed in the residue middle regions) (Fig. 4f). These voids are formed by the bursting of bubbles during the *in situ* expansion process. High magnification SEM micrograph

(Fig. 4g) suggests that the layers are not laterally arranged but are at random. This is a result of the GO particles having different expansion coefficients because of the temperature gradient that exists during the cone calorimeter test. It is also noted that the sample expanded to ~19 mm from the top of the original surface during flame testing despite the majority of blowing/expansion processes occurred *in situ* during processing of this material (based on Fig. 2a). This thus indicates that tremendous expansion is possible if used in polymers having lower processing temperatures.

### 3.4.2. XRD analysis

Wide-angle XRD analysis was carried out for all the collected residues to understand the clay/graphite particle structure therein. In addition, high temperature wide-angle XRD of some selected materials was conducted to monitor the evolution of structural changes *in situ*. Fig. 5a shows powder XRD patterns in the $2\theta$ range 1°–30° for organoclay (as-received) at various temperatures. The first peak at $2\theta \sim 4.5°$ (at 25 °C) corresponds to an interlayer spacing of ~1.8 nm, attributed to the stacking of the silicate layers along the (001) or out-of-plane direction. This is due to the intercalation of the alkyl ammonium molecules within the interlayer gallery. At 100 °C, there is no change in the interlayer spacing indicating no disturbance of the original structure. As mentioned in Section 3.2, the degradation of organoclay usually begins at ~180 °C with loss of olefin, and its evolution continues to 500 °C. In line with the thermal stability results, it is found that with further increase in temperature, the (first) peak shifted to higher angles and at 450 °C, $2\theta$ is ~7.0° ($d$-spacing ~1.3 nm) suggesting that most of the intercalated organic content has been decomposed. Taking the thickness of an individual clay layer (completely dehydrated) as 0.7 nm [48], then ~0.58 nm difference corresponds to the carbonaceous matter still intercalated in the clay layers. At 600 °C, this peak is further shifted to higher angles, broadened and its intensity is very low showing that the dehydroxylation process of aluminosilicate has started. These structural changes are very well represented in the XRD pattern of the combustion residues of B2 and B3 (Fig. 5b). The first peak in both B2 and B3 is at $2\theta \sim 7.0°$, suggesting the collapse of delaminated nanostructures of clay present prior to burning irrespective if POSS is present or not. Similar observations were reported in previous studies [8,9] including our own [10] inferring the same nature of the residue regardless of the matrix, structure of the original nanocomposite (exfoliated or intercalated), loading and the presence of an additional dispersed filler. Hence, this spacing is a thermodynamically stable form of the clay–carbon material produced by thermal degradation.

The second major peak at $2\theta \sim 20.0°$ (an interlayer spacing ~0.44 nm) in both high temperature XRD curves of as-received organoclay (Fig. 5a) and XRD curves of combustion residues of B2 and B3 (Fig. 5b) is assigned to the diffraction from the (110) and (020) planes of the montmorillonite crystal [10,49], both of which are perpendicular to the (001) plane. The third major peak at $2\theta \sim 27.6°$ (corresponding to an interlayer spacing ~0.32 nm) is observed in both residues of B2 and B3, and also in the XRD patterns of organoclay taken at temperatures 350, 450 and 600 °C. This is close to the ordered graphite spacing of 0.335 nm [50]; and

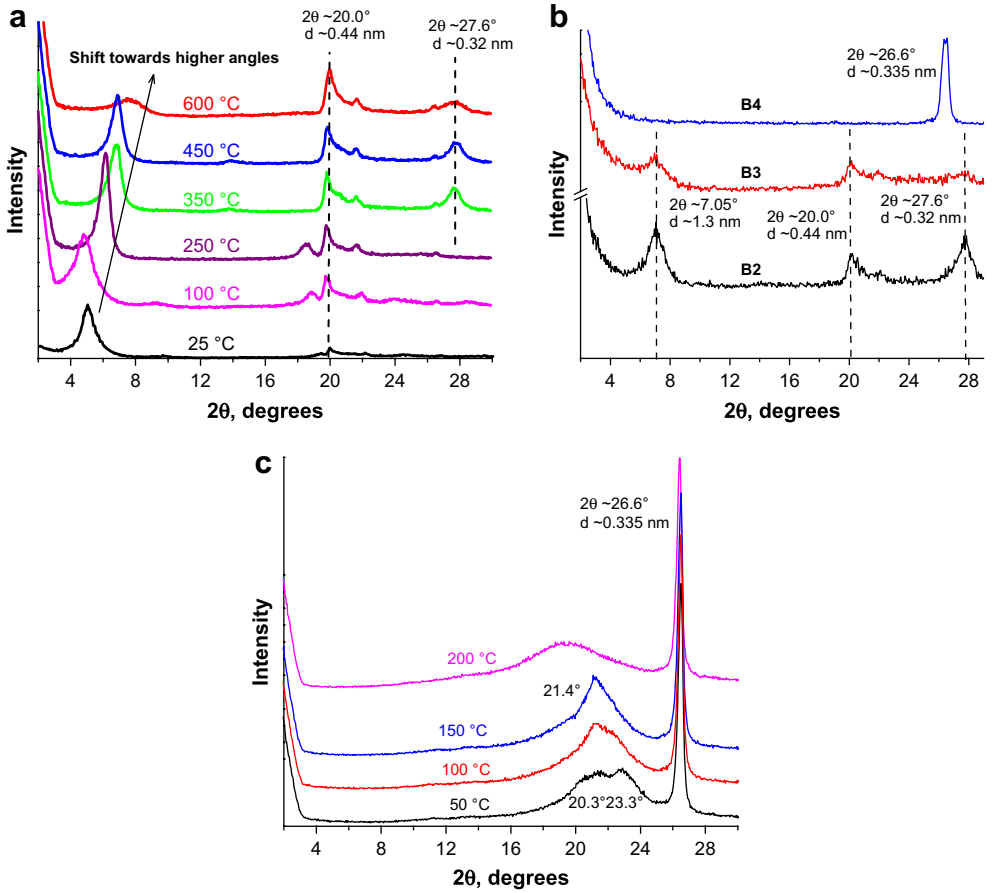


**Fig. 5.** (a, c) X-ray diffraction patterns at various temperatures on: (a) organoclay powder and (c) polyamide 6/GO composite; (b) conventional X-ray diffraction patterns taken on the top surfaces of the residues left after the flame tests for B2 to B4.

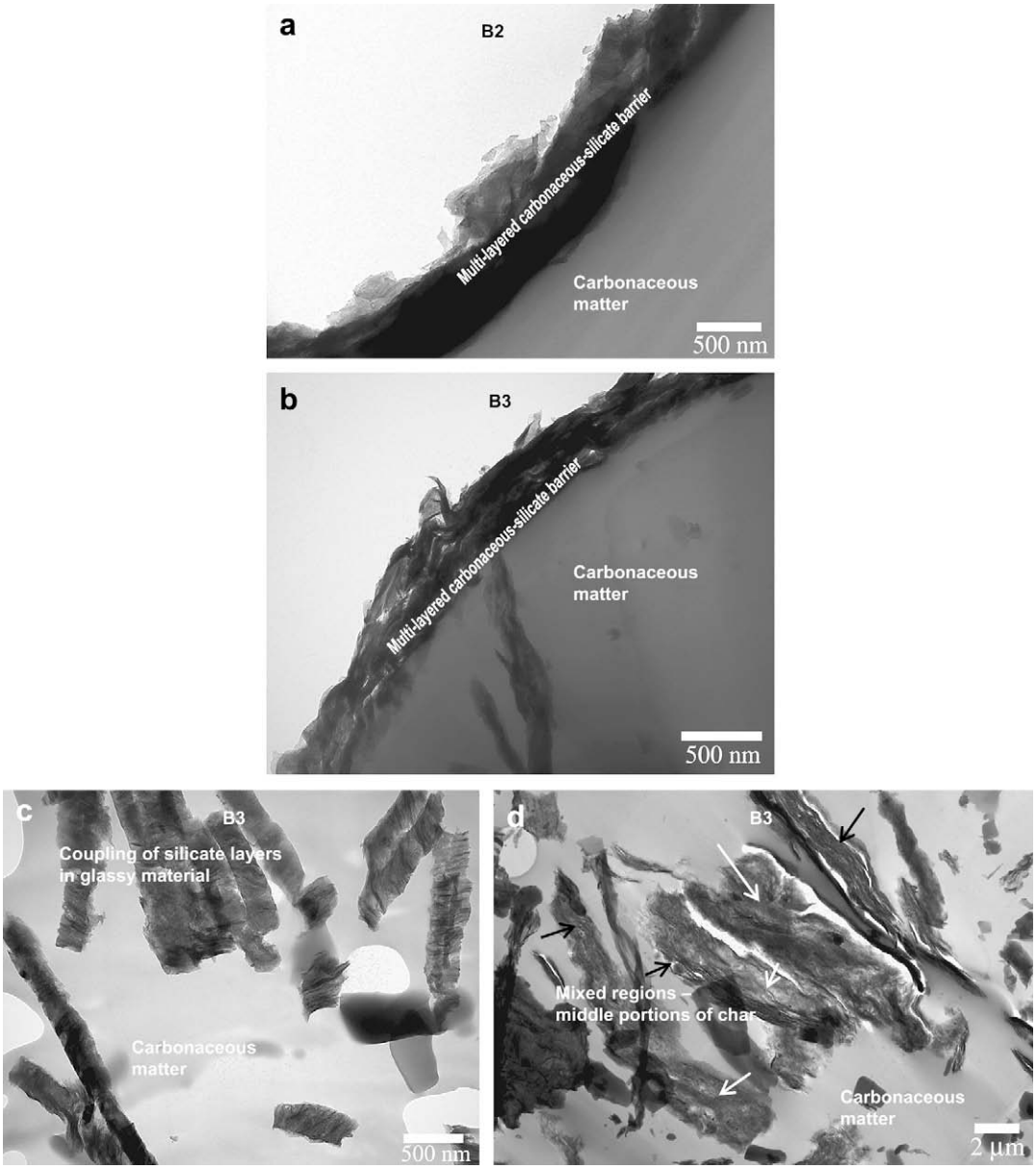


**Fig. 6.** TEM micrographs of cross-sections beneath: (a–c) top, and (d) middle portions of combustion residues of (a) B2 and (b–d) B3. The holey formvar film underneath the sections can also be seen in some cases. The black arrows in (d) point to the multi-layered carbonaceous-silicate barrier; while white arrows indicate a different packing of silicate layers (coupled with glassy material).

more precisely it is the (002) peak for origami graphite [51]. Hence, post-combustion, the organoclay tends to form a thermally stable organic component possibly having a graphitic structure. This peak, however, was previously thought to be a result of the combustion of polymer in the presence of clay [8–10]. But the high temperature XRD curves reveal that this peak exists even in the absence of polymer and is a result of the decomposed organic matter intercalated inside the clay layers. So, in brief, this multi-layered carbonaceous-silicate structure may act as an insulator and mass transport barrier, slowing down the escape of volatile products generated during decomposition. In the residue of B3, it is also noted that no crystalline POSS peaks are seen, which are present before burning. This confirms that POSS cage degradation has occurred and the material has converted from crystalline to amorphous state (glassy char).

For GO, the XRD pattern at ambient temperature (~25 °C) reveals a sharp and high intensity (002) graphite peak at $2\theta \sim 26.6^\circ$ and a broad low intensity peak at $2\theta \sim 13.6^\circ$ (see Section 2.1). Although high temperature XRD analysis was conducted on the GO powder at varying temperatures (100, 250, 350, 450 and 600 °C), the XRD data may not be reliable due to the *in situ* voluminous expansion occurring around 200–250 °C, which may affect the precision of the peak positions. However, high temperature XRD analysis of polyamide 6/GO composite (B4) was conducted at temperatures of 50, 100, 150 and 200 °C and shown in Fig. 5c (due to machine limitations, the experiment was stopped before melting of polyamide 6, which is ~220 °C). The two characteristic crystalline diffraction peaks of (100) and (010, 110) at $2\theta \sim 20.3^\circ$ and $23.3^\circ$ correspond to the α-crystalline phase of polyamide 6 (triclinic form). With increasing temperature, the two peaks move towards each other, and a substantial change in structure occurs at 150 °C. A new diffraction peak at $2\theta \sim 21.4^\circ$ is observed, suggesting that the structure is modified to the γ-form, which is a pseudo-hexagonal phase of polyamide 6. This phenomenon is the well-known Brill

transition of polyamide 6 and can be attributed to the thermal expansion of crystalline lattice; that is, γ-form is favorable at high temperatures. With further increase in temperature to 200 °C (close to the melting temperature of polymer), the intensity of the γ-peak starts to disappear and only a broad peak is seen, and it is slightly shifted to lower angles, which agrees with Liu et al. [52]. Apart from the crystalline peaks of polyamide 6, only a sharp and intense peak corresponding to (002) graphite at $2\theta \sim 26.6^\circ$ is observed at all temperatures studied indicating no changes to the graphitic structure at the temperatures investigated. The combustion residue of B4 yielded the same result showing only one sharp peak at $2\theta \sim 26.6^\circ$ (Fig. 5b). The absence of a peak at $2\theta \sim 27.6^\circ$ also supports the results of high temperature XRD on the organoclay powder.

### 3.4.3. TEM analysis

The combustion residues of B2 and B3 were further examined by cross-sectional TEM (beneath their surfaces) to understand the char morphologies and their role in affecting the flame performance of these materials. As the residue of B4 is extremely soft to handle, TEM studies on this material were not conducted. In B2 (Fig. 6a), the thickness of the protective silicate barrier is ~0.50–0.70 μm though the packing of layers (indicative of char stability) is not perfect and openings can be seen. Higher magnification of the uniform regions of the protective barrier (not shown here) indicated well-ordered multi-layered arrays of silicate-carbonaceous structure similar to [10]. In general, after the decomposition of the organic surfactant that stabilizes the nanocomposite structure, the clay layers still containing organic debris (decomposed carbonaceous matter) are free to migrate to the burning surface. Several driving forces have been suggested to be responsible for the migration of clay layers and they include rising bubbles, viscosity gradients, and convection forces due to the temperature gradient (which may accelerate the migration of the clay particles in the direction of the heat source). On the contrary, rising bubbles may also push the silicate layers out of the sample. Nonetheless, the results clearly indicate that the migration of all the clay layers from within the sample to the burning surface has not taken place as the bottom and middle regions of the residue still showed evidence of clay layers (not shown here). Finally, this gives apertures/openings in the char with insufficient thickness, which is a major concern and points to a negative aspect of clay as a fire retarding agent.

Fig. 6b–d show typical TEM micrographs of residues of polyamide 6/organoclay/POSS ternary nanocomposite with 15 wt.% each of organoclay and POSS. Although the glassy-residue of POSS is expected to couple all silicate layers to each other and enhance the structural integrity of the char, the multi-layered carbonaceous-silicate protective barrier at the surface is only ~0.3–0.6 μm thick and contains much larger openings than B2. Interestingly, there are some regions which are distinct in the carbonaceous matter and where the packing of silicate layers is different due to the presence of the glassy coupling agent (Fig. 6c). Fig. 6d, taken from the middle portions of the char, also shows mixed regions where some of the clay nanostructures collapsed and formed multi-layered structures, while others showed a different packing like those in Fig. 6c. This is the result of the higher melting/conversion temperature of POSS (cage degradation occurs ~550–680 °C) to glassy material that couples the silicate layers. By the time this process happens, it is obvious that most of the clay layers might have collapsed to form aggregated structures and/or migrated to the burning surface because the melting temperature of the polymer is ~220 °C.

In sum, POSS even with its good thermal stability and ability to convert to a glassy material does not seem to have a positive influence on the flame retardant properties of neat polyamide 6 or polyamide 6/organoclay nanocomposite. While GO, despite its advantageous volume expansion during combustion is ineffective in improving the flame retardancy compared to binary polymer/clay nanocomposites. Even discounting the negative effect of the processing temperature of polyamide/GO composites, the residue is extremely soft and it also seems from the XRD curves that GO is directly releasing the oxidant inside the particles instead of exfoliating them. These factors are definitely not beneficial from the viewpoints of safety (the residue softness may result in the quick collapse of a structure) and eco-friendliness (direct release of oxidants is obviously harmful). Considering these factors, it is clear that clay is preferred to GO in polymers because of its eco-friendliness and stability/rigidity of the combustion residue.

Nonetheless, for short-term fire exposure conditions (UL94), it seems that GO is a perfect candidate and many studies, for example [35,53], have shown a V-0 rating with GO as a filler. This is still a problem and not achievable with organoclay. Again POSS due to its higher melting/conversion temperature is not preferred as a coupling agent. Especially, for short-term exposure conditions, this is highly disadvantageous. It is therefore necessary to use a low melting ceramic material to effectively facilitate its beneficial properties. Hence, significant future efforts are still required to enhance the flame performance of polymer nanocomposites containing layered fillers since there was no stage during the cone calorimeter tests where *the peak HRR was further reduced* or *the combustion delayed* compared to the binary clay nanocomposites. Yet these are necessary conditions for the safety of humans and the environment.

## 4. Conclusions

To understand and develop environmental benign and superior flame retardant polymer nanocomposites, two approaches were adopted: (i) additional incorporation of POSS in polyamide 6/organoclay nanocomposites to enhance the char quality and (ii) intumescent polyamide 6 composite using GO to benefit from its voluminous expansion behavior and suffocate the flame.

- Although the initial (5 wt.%) thermal degradation temperature of POSS reinforced nanocomposites was higher, the maximum (peak) degradation temperatures of all the materials (except those with organoclay) were similar. The fine dispersion of organoclay (important for barrier properties) does not play a dominant role in controlling the thermal stability of the nanocomposites.
- Thermal stability results were poorly reflected by the flammability properties, that is, organoclay (and also GO) reinforced materials showed significant reductions in HRRs and MLRs. No improvements were observed with additional incorporation of POSS in the polyamide 6/organoclay nanocomposite.
- TEM analysis of combustion char of binary organoclay/polyamide nanocomposite revealed that the silicate barrier is only 0.5–0.7 μm thick suggesting the migration of clay layers to the top surface must be significantly improved. The barrier thickness in polyamide 6/POSS/organoclay ternary nanocomposite is also similar to the binary nanocomposite. However, there were some regions in the char where the influence of POSS was observed as the silicate layers were closely organized and seen in a different phase (glassy material).
- The voluminous expansion of GO during combustion of polyamide/GO composite combined with the physical barrier mechanism contributed to the significant reductions of HRR (~60% compared to neat polyamide 6) and MLR, and delayed the burning even slightly better than the organoclay nanocomposites. Though the residue was thicker due to the expansion process, it was extremely soft, which would have a deleterious effect on the structural integrity if used in real-life conditions.

## Acknowledgements

We would like to thank the Australian Research Council (ARC) for continuous support of this research project on '*Polymer Nanocomposites*'. We also acknowledge Mr. Russell Collins of CSIRO Manufacturing & Materials Technology, Ryde, Australia, for assistance with the cone calorimeter experiments and Dr Songlin Liu of Singapore Institute of Manufacturing Technology, for help with injection molding of the samples.

## References

[1] Price D, Anthony G, Carty P. In: Horrocks AR, Price D, editors. Fire retardant materials. Cambridge: Woodhead Publishing Ltd and CRC Press LLC; 2001. p. 10.
[2] Bourbigot S, Duquesne S. J Mater Chem 2007;17(22):2283–300.
[3] Lomakin SM, Zaikov GE. In: Ecological aspects of polymer flame retardancy. The Netherlands: VSP BV; 1999. p. 107.
[4] Lu SY, Hamerton I. Prog Polym Sci 2002;27(8):1661–712.
[5] Costache MC, Heidecker J, Manias E, Camino G, Frache A, Beyer G, et al. Polymer 2007;48(22):6532–45.
[6] Levchik SV, Weil ED. Polym Int 2005;54(1):11–35.
[7] Gui H, Zhang X, Liu Y, Dong W, Wang Q, Gao J, et al. Compos Sci Technol 2007;67(6):974–80.
[8] Gilman JW. Appl Clay Sci 1999;15(1–2):31–49.
[9] Kashiwagia T, Harris Jr RH, Zhang X, Briber RM, Cipriano BH, Raghavan SR, et al. Polymer 2004;45(3):881–91.
[10] Dasari A, Yu ZZ, Mai Y-W, Liu S. Nanotechnology 2007;18(7):445602–11.
[11] Morgan AB. Polym Adv Technol 2006;17(4):206–17.
[12] Zanetti M, Camino G, Mulhaupt R. Polym Degrad Stab 2001;74(3):413–7.
[13] Morgan AB, Bundy M. Fire Mater 2007;31(4):257–83.
[14] Bartholmai M, Schartel B. Polym Adv Technol 2004;15(7):355–64.
[15] Zhang Y, Lee S, Yoonessi M, Liang K, Pittman CU. Polymer 2006;47(9):2984–96.
[16] Zhao Y, Schiraldi DA. Polymer 2005;46(25):11640–7.
[17] Jash P, Wilkie CA. Polym Degrad Stab 2005;88(3):401–6.
[18] Fina A, Tabuani D, Carniato F, Frache A, Boccaleri E, Camino G. Thermochim Acta 2006;440(1):36–42.
[19] Devaux E, Rochery M, Bourbigot S. Fire Mater 2002;26(4–5):149–54.
[20] Bourbigot S, Duquesne S, Jama C. Macromol Symp 2006;233(1):180–90.
[21] Zhang J, Xu R, Yu D. Eur Polym J 2007;43(3):743–52.
[22] Zeng J, Bennett C, Jarrett WL, Iyer S, Kumar S, Mathias LJ, et al. Compos Interfaces 2005;11(8–9):673–85.
[23] Fu BX, Namani M, Lee A. Polymer 2003;44(25):7739–47.
[24] Pittman CU, Li GZ, Ni H. Macromol Symp 2003;196(1):301–25.
[25] Liu L, Hu Y, Song L, Nazare S, He S, Hull R. J Mater Sci 2007;42(12):4325–33.
[26] Carniato F, Boccaleri E, Marchese L, Fina A, Tabuani D, Camino G. Eur J Inorg Chem 2007;(4):585–91.
[27] Horacek H, Pieh S. Polym Int 2000;49(10):1106–14.
[28] Wang J, Han Z. Polym Adv Technol 2006;17(4):335–40.
[29] Zhang R, Hu Y, Xu J, Fan W, Chen Z, Wang Q. Macromol Mater Eng 2004;289(4):355–9.
[30] Shi L, Li ZM, Xie BH, Wang JH, Tian CR, Yang MB. Polym Int 2006;55(8):862–71.
[31] Li Z, Qu B. Polym Degrad Stab 2003;81(3):401–8.
[32] Modesti M, Lorenzetti A, Simioni F, Camino G. Polym Degrad Stab 2002;77(2):195–202.
[33] Camino G, Duquesne S, Delobel R, Eling B, Lindsay C, Roels T. In: Nelson GL, Wilkie CA, editors. Fires and polymers: materials and solutions for hazard prevention. Washington, DC: ACS Publishers; 2001. p. 90.
[34] Xie R, Qu B. Polym Degrad Stab 2001;71(3):395–402.
[35] Shih YF, Wang YT, Jeng RJ, Wei KM. Polym Degrad Stab 2004;86(2):339–48.
[36] Li G, Wang LC, Toghiani H, Daulton TL, Koyama K, Pittman CU. Macromolecules 2001;34(25):8686–93.
[37] Liang KW, Li G, Toghiani H, Koo JH, Pittman CU. Chem Mater 2006;18(2):301–12.
[38] Gilman JW, Awad WH, Davis RD, Shields J, Harris Jr RH, Davis C, et al. Chem Mater 2002;14(9):3776–85.
[39] Xie W, Gao Z, Pan WP, Hunter D, Singh A, Vaia R. Chem Mater 2001;13(9):2979–90.
[40] Yu ZZ, Hu GH, Varlet J, Dasari A, Mai Y-W. J Polym Sci Part B Polym Phys 2005;43(9):1100–12.
[41] Hasegawa N, Okamoto H, Kato M, Usuki A, Sato N. Polymer 2003;44(10):2933–7.
[42] Morgan AB, Chu LL, Harris JD. Fire Mater 2005;29(4):213–29.
[43] Weiss A. Angew Chem Int Ed 1981;20(10):850–60.
[44] Kashiwagi T, Grulke E, Hilding J, Groth K, Harris Jr RH, Butler K, et al. Polymer 2004;45(12):4227–39.
[45] Fina A, Bocchini S, Camino G. Polym Degrad Stab 2008;93(9):1647–55.
[46] Qu B, Xie R. Polym Int 2003;52(9):1415–22.
[47] Wang J, Han Z. In: Wilkie CA, Nelson GL, editors. Fire and polymers: materials and concepts for hazard prevention. ACS Symposium Series, vol. 922. Oxford: Oxford University Press; 2005. p. 172.
[48] Sonobe N, Kyotani T, Tomita A. Carbon 1988;26(4):573–8.
[49] Takahashi S, Taniguchi M, Omote K, Wakabayashi N, Tanaka R, Yamagishi A. Chem Phys Lett 2002;352(3–4):213–9.
[50] Reznik D, Olk CH, Neumann DA, Copley JRD. Phys Rev B 1995;52:116.
[51] Ebbesen TW, Hiura H. Adv Mater 1995;7(6):582–6.
[52] Liu X, Wu Q, Zhang QX, Berglund LA, Mo Z. Polym Bull 2002;48(4–5):381–7.
[53] Shi L, Li ZM, Yang MB, Yin B, Zhou QM, Tian CR, et al. Polym Plast Technol Eng 2005;44(7):1323–37.